CHAPTER 4

INVESTIGATIONS ON STRUCTURAL, OPTICAL AND MAGNETIC PROPERTIES OF Mn DOPED ZnO PREPARED BY SOL-GEL METHOD

4.1 INTRODUCTION

In previous chapter, we studied Co doped ZnO with different Co concentrations. In this Chapter, we have investigated the influence of different Mn concentrations on structural, optical and magnetic properties of ZnO. Zinc oxide has attracted the researchers towards extensive studies of its properties with different doping materials [117]. Different groups have reported that Mn doping significantly manipulate the magnetic properties of ZnO [118-119]. In addition to its semiconducting properties, this creates a special attention of this class of materials for the use as diluted magnetic semiconductors (DMS). Such kind of DMS has potential application in magneto-electronics and spintronic devices, which exploit both the electron spin in magnetic materials and the charge of electron in semiconductors. In case of DMS, magnetic properties can be control by type of carrier, their mobility and density. The optical and magnetic properties of the materials can be tuned by tailoring the particle size [120]. Some groups have observed different magnetic behaviour of Mn doped ZnO due to different preparation methods [121-122]. *Dietl et al.* predicted ferromagnetism with a very high Curie temperature in *p* type ZnO and GaN [123]. The paramagnetic behaviour has been observed in Mn doped bulk ZnO prepared by solid state reaction technique [124]. *Luo et al.* found an anti-ferromagnetic ordering in Mn doped ZnO nanoparticles prepared by a combustion method [125]. However, the correct mechanism of room temperature ferromagnetism (RTFM) is still a topic of debate. Also, substitution of Mn ions in host semiconductor may produce small lattice disorder or defects, which is

responsible for change in structural, optical and magnetic properties of host semiconductor.

In this chapter we present the study on structure, morphology, elemental analysis, Raman scattering, FTIR, optical and magnetic properties of sol-gel derived Mn doped ZnO nanopowder. UV-Vis analysis has been performed to know the effect of Mn concentrations on absorption properties of ZnO. These results show strong absorption broadening with Mn doping in UV region with absorption edge in visible region, which may have important application for photo-detector or solar cell. RTFM is important for practical spintronic devices, therefore we have also studied magnetic properties of samples to know the effect of Mn concentrations on RTFM. In this study we have tried to correlate the change in absorption and RTFM of samples with structural change due to Mn incorporation using an easier rout of synthesis.

4.2. EXPERIMENTAL PROCEDURE

4.2.1 Synthesis of ZnO: Mn Nanoparticles

The samples of Mn doped ZnO with nominal compositions $Zn_{1-x}Mn_xO$ (x= 0.00, 0.02, 0.04 and 0.06) have been synthesized by sol gel route using high purity analytical grade acetates of Zn and Mn i.e. $Zn(CH_3CO_2)_2.2\ H_2O$ and $Mn(CH_3CO_2)_2.4H_2O$ without any further purification. For the synthesis of the samples, we dissolved appropriate amount of zinc acetate dehydrate in isopropyl alcohol under magnetic stirring for 2h and then added appropriate proportion of manganese acetate tetra hydrate with stirring until complete dissolution of the precursors. Moreover, urea was used as a burning agent and then, the resultant solution was stirred until the gel was obtained. In this entire process the temperature was maintained at 100° C. These gels were then heated at 500°C for 30 min in furnace to obtain sample in powder form. An additional heat treatment was given at 600°C for two hours in furnace to remove the impurities. Then samples in pellets form

were placed in crucible for sintering in furnace at 1000°C for two hours followed by furnace cooling to room temperature. Further pellets have been crushed to get powder sample for all characterisations while EDS and SEM characterisation have performed in pellets form with gold coating on the samples.

4.2.2 Characterisations

The phase confirmation of synthesized samples has been performed by Rigaku-MiniFlex-II DESKTOP powder X-ray diffractometer with CuK_α radiation (λ= 1.54 Å) at 30kV and 15mA. All patterns were recorded over the range $20^o \leq 2\theta \leq 80^o$ with a step size of 0.02º. The morphology has been investigated with scanning electron microscope (SEM) in pellets forms. OXFORD Instrument SEM EVO 18 Research has been used for SEM and EDS analysis. The optical absorption spectra of the samples have been recorded by the Lambda–35 UV-Vis spectrophotometer from PerkinElmer in the range of 200-800 nm. The room temperature Raman spectrum ranging from 100 to 1000 cm^{-1} have been collected with a Renishaw in-Via Raman Spectrometer. Fourier Transform Infrared (FTIR-8400S) spectrophotometer has been used to obtain information about functional groups present in the samples. Magnetic behaviour has been measured using Quantum Design MPMS-3 magnetometer in temperature range 5-300 K.

4.3. RESULTS AND DISCUSSIONS

4.3.1 Structural Analysis

X-ray diffraction has been used to estimate structural parameters and phase purity of ZnO and Mn doped ZnO system. Figure 4.1 shows XRD pattern of synthesized $Zn_{1-x}Mn_xO$(x=0.00, 0.02, 0.04 and 0.06) nanopowder. The sharp and intense peaks indicate that the samples are highly crystallite. The XRD peaks for (100), (002), (101), (102), (110), (103) and (112) planes are found to be in a good agreement with the standard peak position of pure ZnO (PDF: 792205). No extra peaks of impurity phases

are detected within the detection limit of the instrument (except x=0.06). It indicates that all the investigated samples have hexagonal wurtzite structure with a space group $P6_3mc$. We have observed some traces of impurity peak of Mn_3O_4 for x=0.06. We should pointed out that volume fraction of Mn_3O_4 in doped ZnO is very small. Thus we can predict that Mn_3O_4 does not significantly affect the properties of ZnO. *S. Kumar et al.* also observed presence of Mn_3O_4 in Mn doped ZnO [36]. It has been observed that peak position of planes shifted towards higher angles and lower intensities with Mn concentration increasing, which causes small variation in lattice parameters. Figures 4.2 (a), (b) and (c) show peak position of (100), (002) and (101) planes respectively. These Figures confirm the peak position shift.

The lattice constants and volume of unit cell of ZnO: Mn has been calculated with Unit Cell Software. Values of lattice constants are listed in Table 4.1. The lattice constant '*a*' of Mn doped ZnO is slightly larger than those of un-doped ZnO because the ionic radius of Mn^{2+} (0.80 Å) is slightly larger than that of Zn^{2+} (0.74 Å) ions [119]. The variation of *c/a* ratio with Mn concentration has been shown in Figure 4.3, which indicates that *c/a* ratio decreases with the increase of Mn concentration. This indicates the occurrence of lattice distortion with Mn concentration.

For HCP structure $a = b \neq c$ and *c/a* =1.633, when Mn^{2+} of higher ionic radius substituted at the place of Zn^{2+} ions, the lattice parameter '*a*' as well as '*b*' increases, which causes decrease in '*c*' in order to maintain distorted HCP structure. Thus *c/a* ratio decreases with increase in Mn concentration. This indicates that crystal structure shift towards higher symmetry. The change in *c/a* ratio with Mn concentration confirms the incorporation of Mn^{2+} ion at Zn^{2+} site of ZnO structure.

The volume of the unit cell has been calculated using the Equation.

$$V = \frac{\sqrt{3}}{2} a^2 c \quad \ldots\ldots\ldots\ldots \qquad (4.1)$$

The values of unit cell volume are listed in Table-1, which shows that volume is changes with Mn concentration. It may be due to variation in lattice constants with Mn concentration.

Atomic packing fraction has been calculated using formula

$$\text{APF} = \frac{2\pi a}{3\sqrt{3}c} \quad \ldots\ldots\ldots\ldots\ldots (4.2)$$

Where '*a'* and '*c'* are lattice parameter.

Figure 4.4 shows the variation of APF with Mn concentration and its values are listed in Table 4.1.The observed value of APF is approximately 75%, while APF of bulk ZnO is nearly 74%, which indicates that APF of investigated samples are slightly larger than bulk ZnO. It may be due to size effect in samples. APF increases with the increase of Mn concentration, which may be because of decrement of voids in the samples. The crystallite size of pure and Mn doped ZnO have been calculated using Scherer's formula [101] (Equation 3.1). The crystallite size of undoped sample is higher initially and latter it decreases for Mn(2%) doping as the lattice easily accept Mn^{2+} ions without affecting ZnO structure. As Mn concentration starts increasing, crystallite size increases as shown in Figure 4.5. The same behaviour has been obtained by *B.N. Dole et.al.*[91]. Change in crystallite size with Mn concentration attributed to substitution of Mn^{2+} ion in Zn^{2+} site of ZnO structure, as incorporation of Mn^{2+} ions (having higher ionic radius than Zn^{2+}) in ZnO structure can create some strains/stress, which in turn can promote both densification and grain growth and can increase grain boundaries or surface diffusion etc.

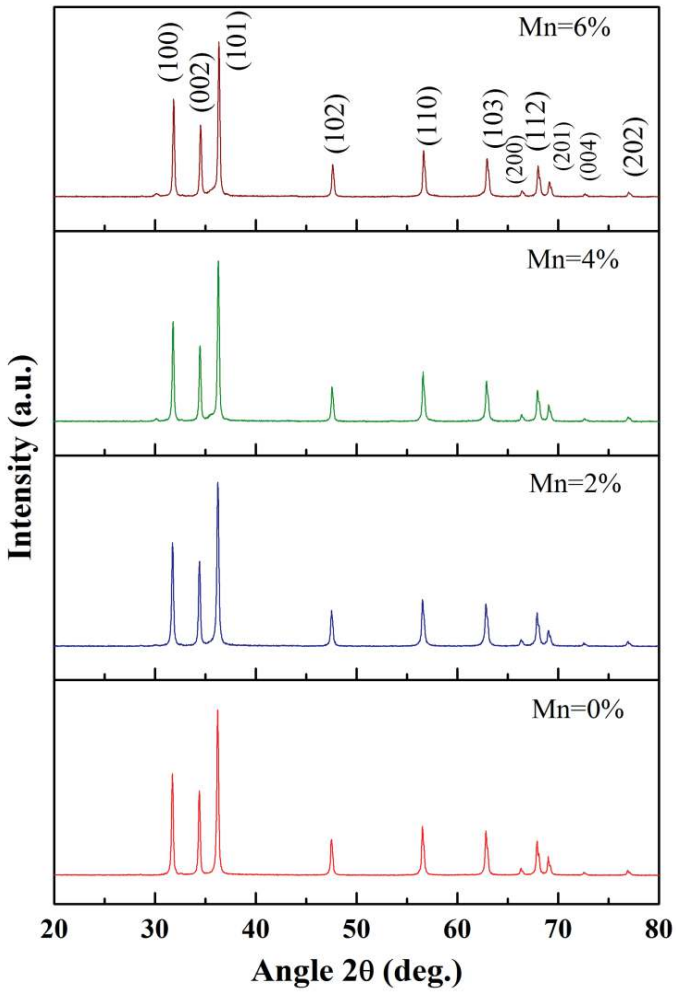

Figure 4.1: XRD pattern of $Zn_{1-x}Mn_xO$ (0.00, 0.02, 0.04 and 0.06) sintered at 1000°C.

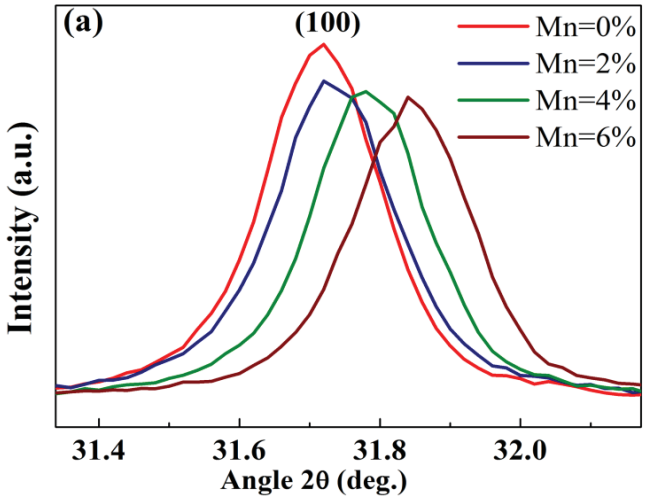

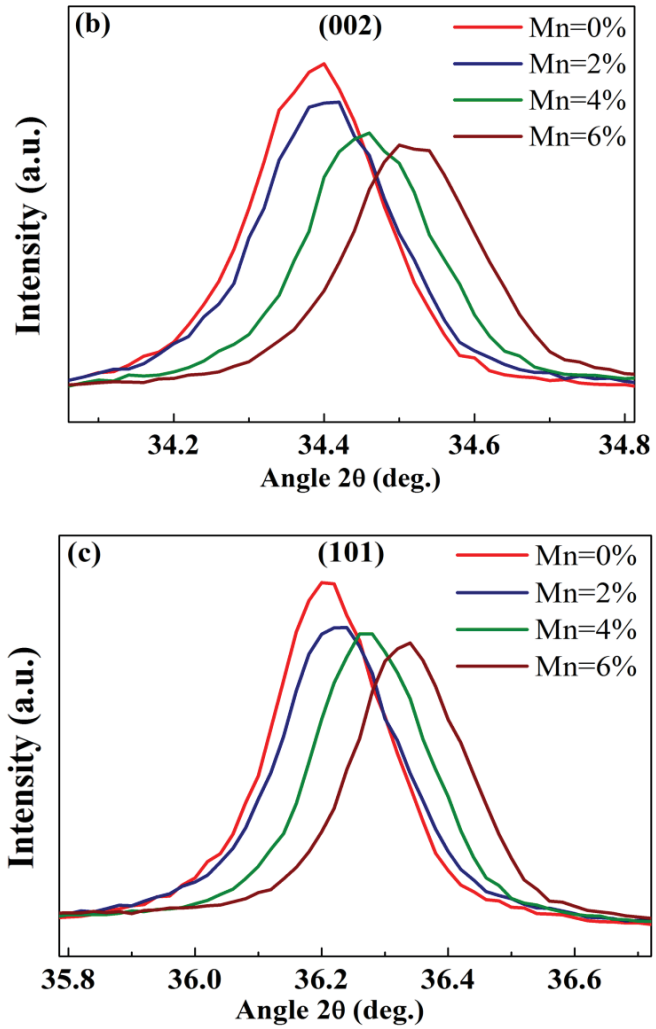

Figure 4.2: (a), **(b)** and **(c)** shows peak position of (100), (002) and (101) planes respectively.

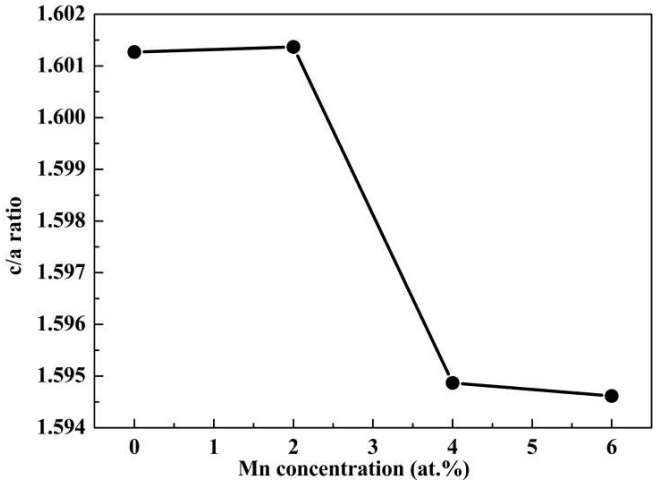

Figure 4.3: The variation of lattice parameters ratio (c/a) with Mn concentration.

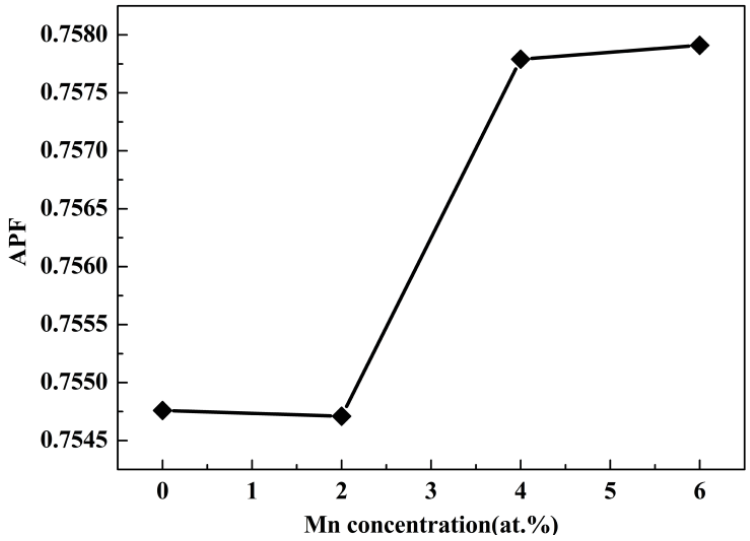

Figure 4.4: Variation of APF with Mn concentration.

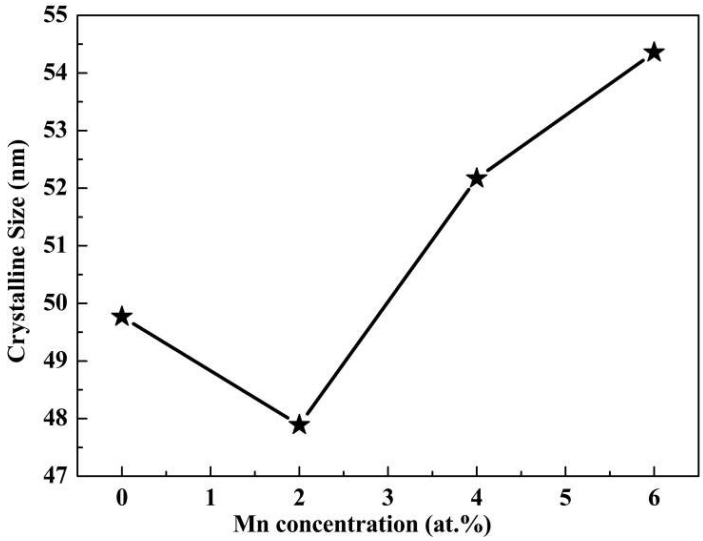

Figure 4.5: Change in crystalline size with Mn concentration.

Table 4.1. The lattice parameter, crystallite size, cell volume and atomic packing fraction of the samples.					
Composition	Lattice parameter		Crystallite size (nm)	Cell volume $(Å)^3$	APF
	a(Å)	c(Å)			
ZnO	3.2533	5.2093	49.76	47.7470	0.7548
$Zn_{.98}$ $Mn_{.02}O$	3.2529	5.2091	47.88	47.7346	0.7547
$Zn_{.96}$ $Mn_{.04}O$	3.2671	5.2105	52.17	48.1646	0.7578
$Zn_{.94}$ $Mn_{.06}O$	3.2644	5.2055	54.35	48.0403	0.7579

4.3.2 Morphological Analysis

We have done SEM characterization to study the morphology (texture), crystallite structure, grain size and orientation of materials making up the sample. SEM micrographs of samples under investigation are shown in Figure 4.6(a-d), which confirms the crystallite structure of $Zn_{1-x}Mn_xO$ (x= 0.00, 0.02, 0.04 and 0.06) nanopowder. From image analysis it has been observed that crystallites are fused to form grains. The grain size calculated by SEM micrograph indicates that most of the grains are in the range of 200-300nm for all samples under investigation.

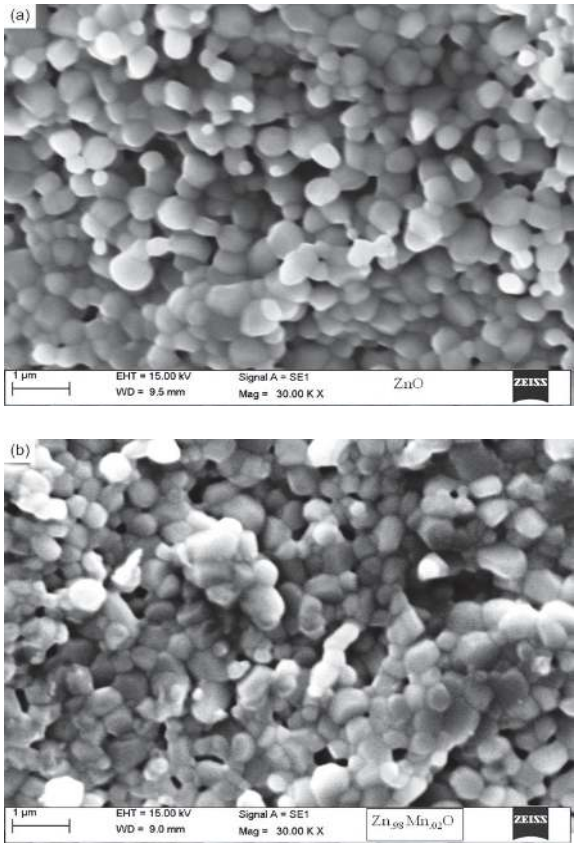

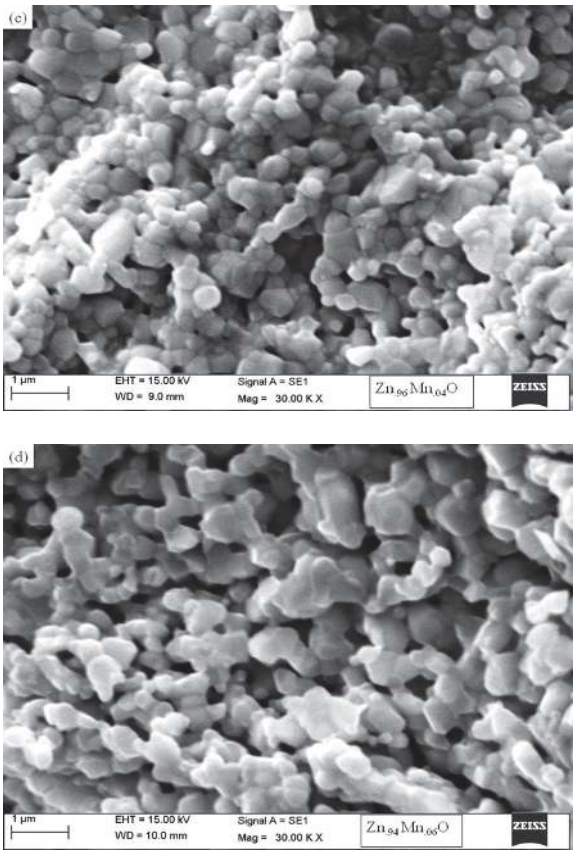

Figure 4.6: SEM image of **(a)** ZnO, **(b)** $Zn_{0.98}$ $Mn_{0.02}O$, **(c)** $Zn_{0.96}$ $Mn_{0.04}O$ and **(d)** $Zn_{0.94}Mn_{0.06}O$ nanopowder respectively.

4.3.3 EDS Analysis

Energy dispersive X-ray spectroscopy has been used for qualitative and quantitative analysis of the entire element present in the samples. Image of SEM micrograph shows particular region of EDS analysis. Elemental mapping for distribution and relative proportion of $Zn_{0.98}$ $Mn_{0.02}O$ over the scanned area are shown in Figure 4.7. Same process has been used for all the samples. The ratio of Zn: Mn: O has been given in Table 4.2, which confirms the presence of Mn in ZnO structure. It has been observed that atomic and weight percentage of Mn within the scanned area increases with increase in doping concentration.

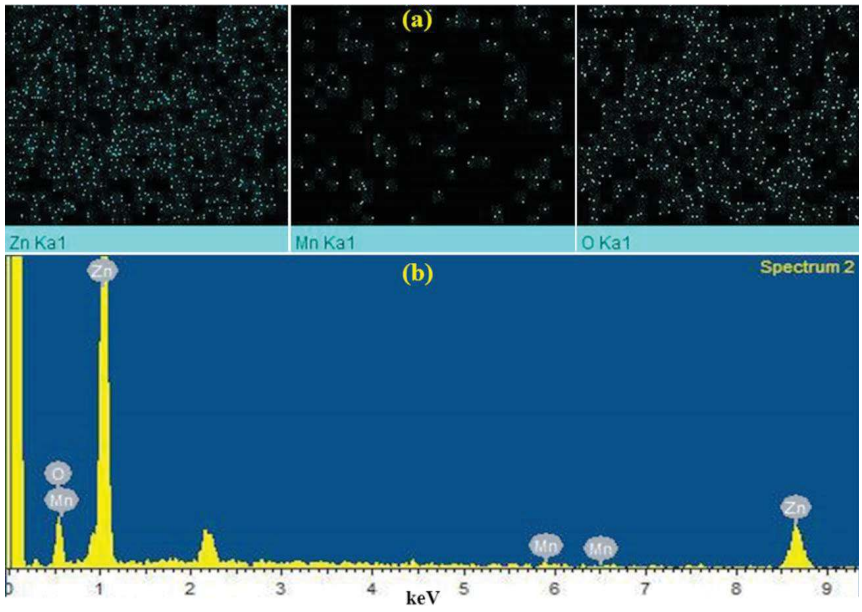

Figure 4.7: EDS spectra of Mn doped ZnO nanopowder.

Table 4.2: Atomic and weight percentage of all the samples.

Mn %	Zn		Mn		O	
	Atomic %	Weight %	Atomic %	Weight %	Atomic %	Weight %
0	49.50	80.02	0	0	50.5	19.98
2	56.77	83.48	1.11	1.37	42.12	15.16
4	51.09	79.33	2.25	2.93	46.66	17.73
6	50.92	78.15	3.74	4.82	45.34	17.03

4.3.4 Optical Properties

Absorption spectroscopy is a powerful technique to explore the optical properties of nanoparticles. The absorption spectra that measured in the range of 200-800nm of the ZnO and Mn doped ZnO nanoparticles at different concentration of Mn (0, 2, 4 and 6%) are presented in Figure 4.8. The absorption curves exhibit an intensive absorption in 200-380 nm wavelength range, with the absorption edge between 400-550 nm. From this result it is clear that absorption edge shifted towards higher wavelength with the increase of Mn concentration. In best of our knowledge, no one has reported encroachment in visible region up to 550 nm with Mn doped ZnO nanoparticles without secondary phase

formation. *A. Abdel-Galil et al.* reported absorption in visible region due to formation of flower like structure [126]. *K. Omri et al.* reported absorption edge between 300 and 370 nm [127]. *R. L. Orimi et al.* has observed absorption in visible region due to secondary phase formation [128]. Some authors have reported blue shift in Mn doped ZnO due to quantum confinement or orbital's hybridization [129]. The absorption edge shift in the considered samples may be due to surface effect/average crystallite size or morphology. This indicates substitution of Mn ions into the Zn site of ZnO lattice. The change in band gap is also responsible for absorption edge shift of samples. In order to find the effect of Mn concentration on band gap, we made use of Tauc relation (Equation 3.2) to calculate optical band gap [104].

Tauc plot to calculate band gap of individual samples have been shown in Figure 4.9(a-d). It has been found that the band gap energy decreases with the increase of doped Mn concentration up to 4%. The decrease in band gap with increase in Mn concentration is also reported by different authors [127] . It may be due to the sp-d exchange interaction between transition metal ions and Zn or due to Mn clustering, changing in average crystallite size and surface area to volume ratio. The band gap of $Zn_{1-x}Mn_xO$ (x=0.00, 0.02, 0.04 and 0.06) have been in the range of 3.00–2.85eV. The variation of band gap with Mn concentration is shown in Figure 4.10. The ferromagnetism in Mn doped ZnO is due to localized magnetic moments mediated by free charge carriers. The Magnetisation curve shows magnetic behaviour increases with Mn concentrations, this indicates increase in the charge carriers with Mn doping. This increase in charge carriers affects the sp-d exchange interactions by increasing *d* electron moments of Mn ions, which could results the red shift in the band gap. Thus, the magnetic behaviour of samples also affects the band gap of materials. The blue shift in the band gap has been explained with the help of Burstein Moss effect [101,117]. In case of Burstein Moss effect Fermi level merges in to

conduction band due to increase of carrier concentration. But in our observation band gap decreases up to 4% doping and then a small increase for 6% doping. This type of behaviour has also been observed by *S. V. Bhat et al.* [130]. The initial decrease of band gap, followed by an increase is termed as band gap "Bowing". This type of band gap bowing has also been observed in Mn doped ZnO thin film, nanoparticles and Mn doped CdS [131]. The band gap bowing has been theoretically explained using second order perturbation theory [132]. *H. Shi et al.* observed that bowing parameter for ZnBeO and MgBeO alloys are large and dependent on composition [133]. Therefore, observed variation of band gap may be due to sp-d exchange interactions affected by the composition.

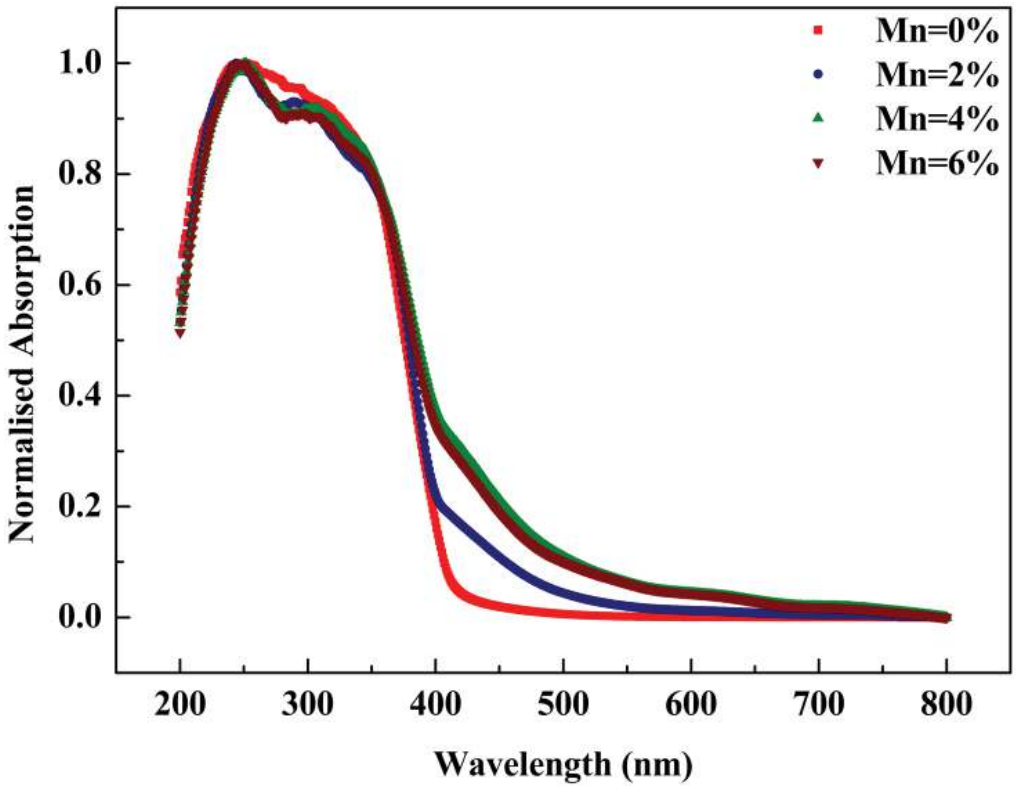

Figure 4.8: Absorption Spectra of $Zn_{1-x}Mn_xO$ nanopowder.

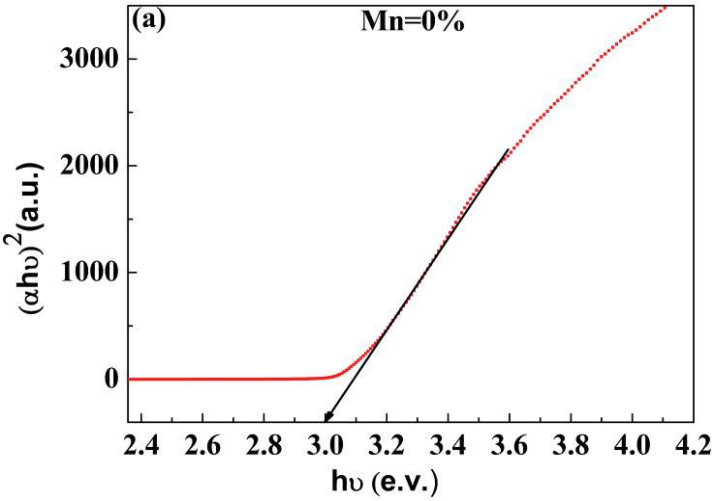
(a)
Mn=0%
3000
2000
1000
0
(αhυ)2(a.u.)
2.4 2.6 2.8 3.0 3.2 3.4 3.6 3.8 4.0 4.2
hυ (e.v.)

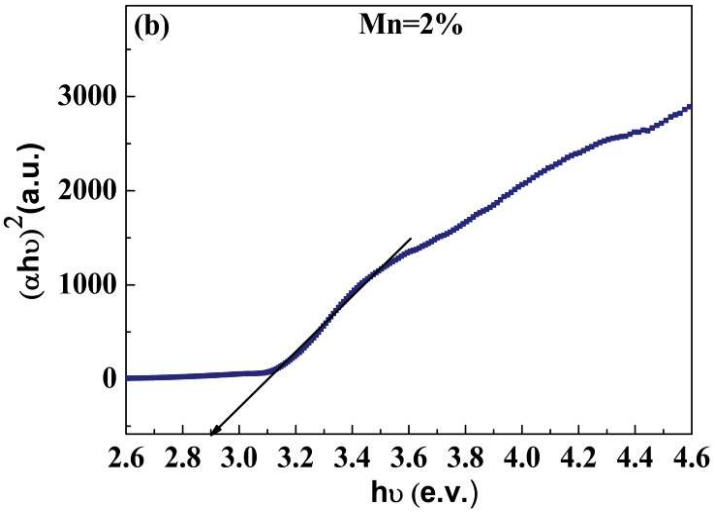
(b)
Mn=2%
3000
2000
1000
0
(αhυ)2(a.u.)
2.6 2.8 3.0 3.2 3.4 3.6 3.8 4.0 4.2 4.4 4.6
hυ (e.v.)

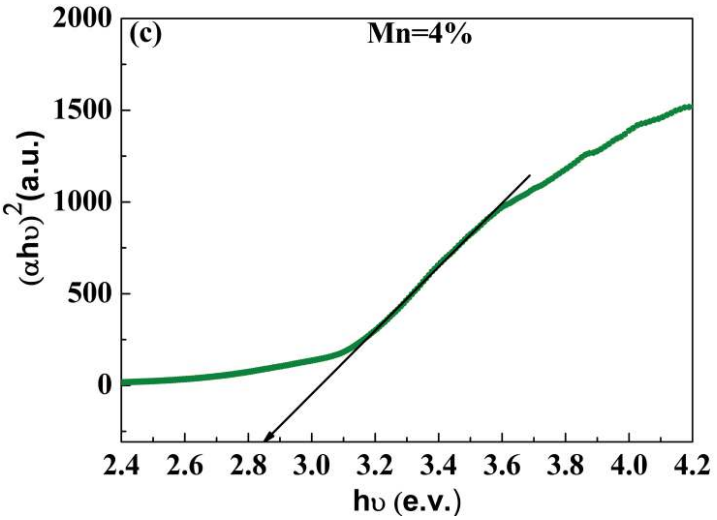
(c)
Mn=4%
2000
1500
1000
500
0
(αhυ)2(a.u.)
2.4 2.6 2.8 3.0 3.2 3.4 3.6 3.8 4.0 4.2
hυ (e.v.)

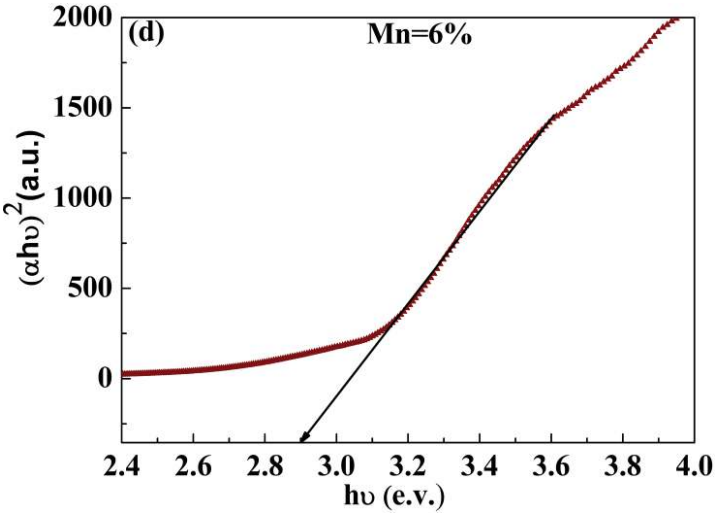

Figure 4.9: $(\alpha h\nu)^2$ versus photon energy of **(a)** ZnO, **(b)** $Zn_{0.98}$ $Mn_{0.02}O$, **(c)** $Zn_{0.96}$ $Mn_{0.04}O$ and **(d)** $Zn_{0.94}$ $Mn_{0.06}O$ nanopowder.

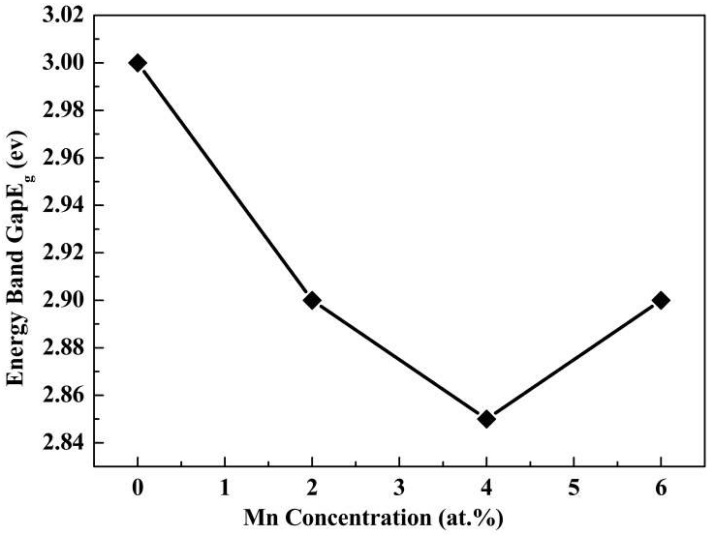

Figure 4.10: Energy band gap versus Mn concentration of $Zn_{1-x}Mn_xO$ nanopowder.

4.3.5 Raman Analysis

Raman spectra are recorded at room temperature to investigate micro-structural and vibrational properties of ZnO wurtzite structure. The optical phonon irreducible representation is given by [134]

$$\Gamma_{opt} = A_1 + 2B_1 + E_1 + 2E_2 \quad \ldots\ldots\ldots\ldots (4.3)$$

Where, A_1 and E_1 are polar modes. These modes can split in to transverse optical (TO) and longitudinal optical (LO) phonon. While B_1 mode is Raman inactive. Non-polar raman E_2 active modes have two wave numbers namely E_2^{low} and E_2^{high}, which are associated with motion of oxygen and zinc sub lattice respectively. The wurtzite ZnO nanoparticles have six Raman active phonon modes at 101(E_2^{low}), 381(A_1 TO), 407(E_1 TO), 437(E_2^{high}), 574 (A_1 LO) and 583 cm^{-1} (E_1 LO) respectively [26].

Raman spectra of $Zn_{1-x}Mn_xO$ shown in Figure 4.11 confirms that all the prominent peaks of ZnO are also present in Mn doped ZnO. The two first order modes observed at 98 and 435 cm^{-1} corresponds to E_2^{low} and E_2^{high} of pure ZnO nanopowder. The mode observed at 330 $cm^{-1}$and 539 cm^{-1} is attributed to E_2^{high}- E_2^{low} and E_2^{high}+ E_2^{low} respectively. While 579 cm^{-1} represent A_1 (LO) of first order. Intensity of addition second mode at 539 cm^{-1} increases with Mn concentration and merges with A_1 (LO) phonon. The presence of E_2^{low} and E_2^{high} in all samples under investigation confirms that Mn doping does not change wurtzite structure of ZnO. Raman scattering results are well consistent with those of XRD. Intensity of E_2 modes decreases with increase in Mn concentration that indicates small distortion in ZnO crystal structure due to incorporation of Mn^{2+} ions. Some additional peaks like (138,168 and 680 cm^{-1}) in Mn 2% ; (123,158 and 673 cm^{-1}) in Mn 4% and (124, 163 and 673 cm^{-1}) in Mn 6% have been observed, which may be due to defects induced by Mn ions. The Mn^{2+} and Zn^{2+} induced some defects such as vacancies and interstitials which activate some additional vibration modes. The presence of doping vibration has also observed by *Wang et.al.* [135]. All observed Raman peaks of $Zn_{1-x}Mn_xO$ are tabulated in Table 4.3.

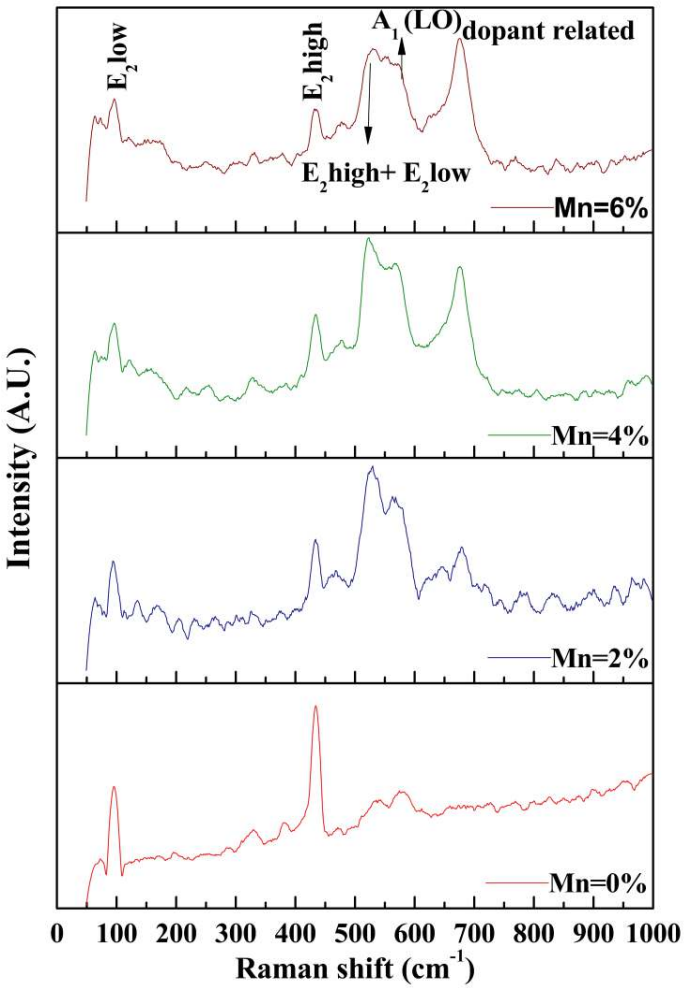

Figure 4.11: Raman spectra of $Zn_{1-x}Mn_xO$ nanopowder at room temperature.

Table 4.3: Observed Raman peak positions of $Zn_{1-x}Mn_xO$ nanoparticles and their assignment				
Vibration Frequency (cm^{-1})				
ZnO	$Zn_{.98}$ $Mn_{.02}O$	$Zn_{.96}$ $Mn_{.04}O$	$Zn_{.94}$ $Mn_{.06}O$	assignments
98	96	95	96	E_2^{low}
	138	123	124	doping related
	168	158	163	doping related
330	327	330	331	E_2^{high}- E_2^{low}
384	376	384	380	A_1 (TO)
435	434	435	435	E_2^{high}
539	531	523	531	E_2^{high}+ E_2^{low}
579	569	566	553	A_1 (LO)
	680	673	673	doping related

4.3.6 FTIR Studies

Fourier Transform Infrared Spectroscopy technique is used to obtain information about functional groups present in the samples, the molecular geometry and inter or intra molecular interactions. We have recorded room temperature FTIR spectra to study the vibrational bands present in $Zn_{1-x}Mn_xO$ samples. Normally, we consider that the band frequencies within 1000 cm^{-1} are associated with the bonds between inorganic elements. FTIR vibrational frequencies for different modes of $Zn_{1-x}Mn_xO$ (x=0.00, 0.02, 0.04 and 0.06) have been shown in Figure 4.12 and listed in Table 4.4. The FTIR vibrational frequencies presenting at 588 cm^{-1}, 675 cm^{-1}, 669 cm^{-1}, 684 cm^{-1} for X=0.00, 0.02, 0.04 and 0.06 concentration respectively are due to Zn-O stretching. This confirms the wurtzite structure formation of the samples [91].

The peak observed at ~1000 cm^{-1} can be attributed to O-H asymmetric stretching mode. The peaks at ~1410 cm^{-1} and~1600 cm^{-1} are assigned to the symmetric stretching of C=O and asymmetric stretching of carboxyl group respectively. Intensity at 1600 cm^{-1} for Mn 2% and Mn 6% are higher as compared to ZnO. The peak around ~2350 cm^{-1} is due to CO_2 molecule present in the acetate and in air. The peak at ~2350 cm^{-1} is disappeared for $Zn_{0.96}Mn_{0.04}O$. It may be possible that samples have trapped some CO_2 from atmosphere during FTIR characterisation. Therefore presences of CO_2 vibrational modes are not serious contamination in $Zn_{1-x}Mn_xO$ nanoparticles. Zn-O stretching modes have a blue shift from 588 cm^{-1} to 684 cm^{-1} with increase in Mn concentrations. The blue shift observed in the samples can be explained on the basis of atomic mass of the atom present in $Zn_{1-x}Mn_xO$. Since Mn (54.93u) has less atomic mass as compared to Zn (65.38u) Mn must have vibrational modes in the higher wave number region. Hence with increase in Mn concentration peak shifted towards higher wave number, which confirms the substitution of Mn ions in Zn site of ZnO nanoparticles.

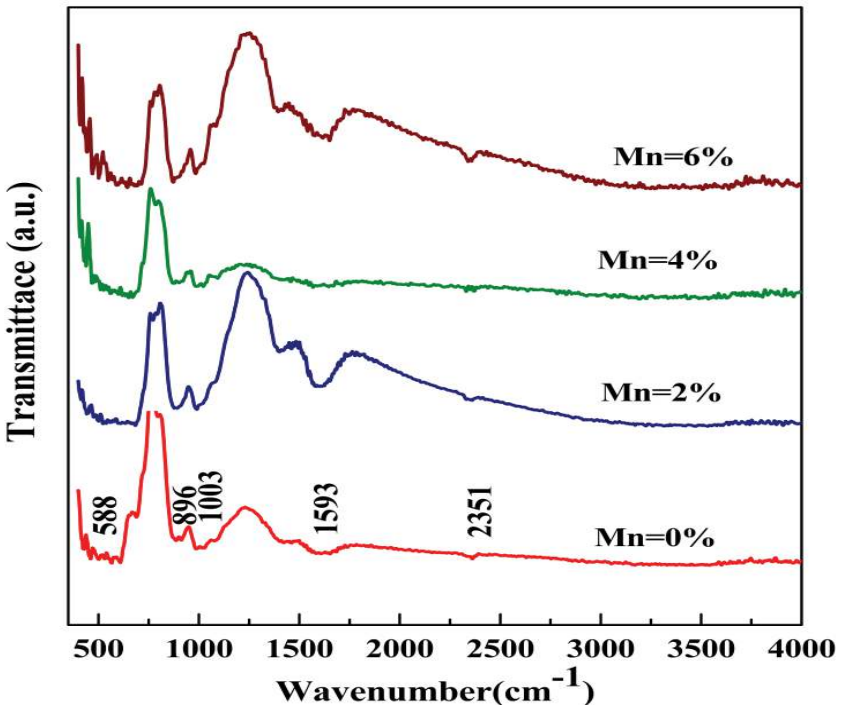

Figure 4.12: FTIR spectra of $Zn_{1-x}Mn_xO$ nanopowder.

Table 4.4: FTIR peak assignments of $Zn_{1-x}Mn_xO$ system.				
Wavenumbers (cm^{-1})				Assignments
ZnO	$Zn_{0.98}Mn_{0.02}O$	$Zn_{0.96}Mn_{0.04}O$	$Zn_{0.94}Mn_{0.06}O$	
588	675	699	684	Zn-O stretching
896	898	900	881	weak vibration of ZnO
1003	1008	1010	995	O-H asymmetric stretching
1410	1410	1406	1410	symmetric stretching of C=O
1593	1599	1609	1626	asymmetric stretching of carboxyl group
2351	2351		2343	Co_2 molecule in Air

4.3.7 Magnetic Property

Figure 4.13 shows the measured room temperature magnetisation curve for the pure and Mn doped ZnO samples. It has been observed that anti-ferromagnetic behaviour is increasing with Mn concentration. Figure 4.14 shows a close scan near the origin for pure ZnO nanopowder. It has been found that coercivity (H_c) and saturation remanence (M_{rs}) for pure ZnO is 168Oe and 0.00846emu/g respectively. These low values of

remanence and coercivity suggest the presence of multi domain magnetisation process. The close scan near origin for Mn doped ZnO shows decrease in coercivity with increase in Mn concentration. The values of coercivity and saturation remanence are listed in Table 4.5. This decrease of the saturation magnetisation with increase in Mn concentration can be attributed to the possible anti-ferromagnetic order between nearest neighbour of Mn – Mn atoms. The distance between Mn ions decreases with increase in number of Mn atoms, will lead to anti-ferromagnetic exchange. Figure 4.15 shows temperature dependence of susceptibility of Mn doped ZnO and inset shows ZFC- FC curve of pure ZnO.

Zero field cooling-field cooling (ZFC-FC) plots for each sample does not show any significant differences. ZFC-FC data lies nearly on the same point in the curve i.e. ZFC-FC curves are identical in nature. All samples exhibit Curie-Weiss behaviour. Curie temperature has been calculated by high temperature linear part of $1/\chi$ verses T curve using Curie- Weiss law. The Curie temperature of $Zn_{1-x}Mn_xO$ (x=0.00, 0.02, 0.04 and 0.06) have been found to be 1257, 269, 111 and 80 K respectively. This indicates a reinforcement of anti-ferromagnetism (AF) with increase in Mn concentration. Metallic Mn and all possible Mn oxides phase like MnO, MnO_2, Mn_2O_3 are anti-ferromagnetic except Mn_3O_4, which is ferromagnetic only below 45K. From Figure 4.15 we can say that susceptibly and magnetisation value decreases with increase of temperature. An abrupt decrease in susceptibility value can be associated to magnetic phase change. This ferromagnetic phase change is due to Mn induced defect incorporation in the system. Although lots of theoretical and experimental works have been done about transition metal doped ZnO [136], the origin of ferromagnetism in $Zn_{1-x}Mn_xO$ is not clear yet. Some authors have reported that it is intrinsic property of system or the concentration of oxygen vacancy is responsible for ferromagnetic exchange between Mn ions. Other authors

suggested that ferromagnetism in Mn doped ZnO is due to secondary phase formation like $ZnMn_2O_4$, Mn_3O_4 etc.[119]. *Coey et al.* observed that ferromagnetic exchange in dilute ferromagnetic oxide can be mediated by shallow donor electron [137] . In our case XRD result confirm that there is no any secondary phase present in the system except in Mn 6%. Therefore we believe that ferromagnetism in our case is due to defect and incorporation of Mn in ZnO host. The connection between structural defect and RTFM has been studied by several authors [135]. In our study, E_2 mode in Raman spectra become weak with increase in Mn concentration, which indicates that ZnO crystal structure, is destroyed gradually by substitution of Mn ions. XRD result also support that lattice distortion takes place with increase in Mn concentration. Thus our study has clearly shown that defect is an important factor affecting the RTFM of ZnO.

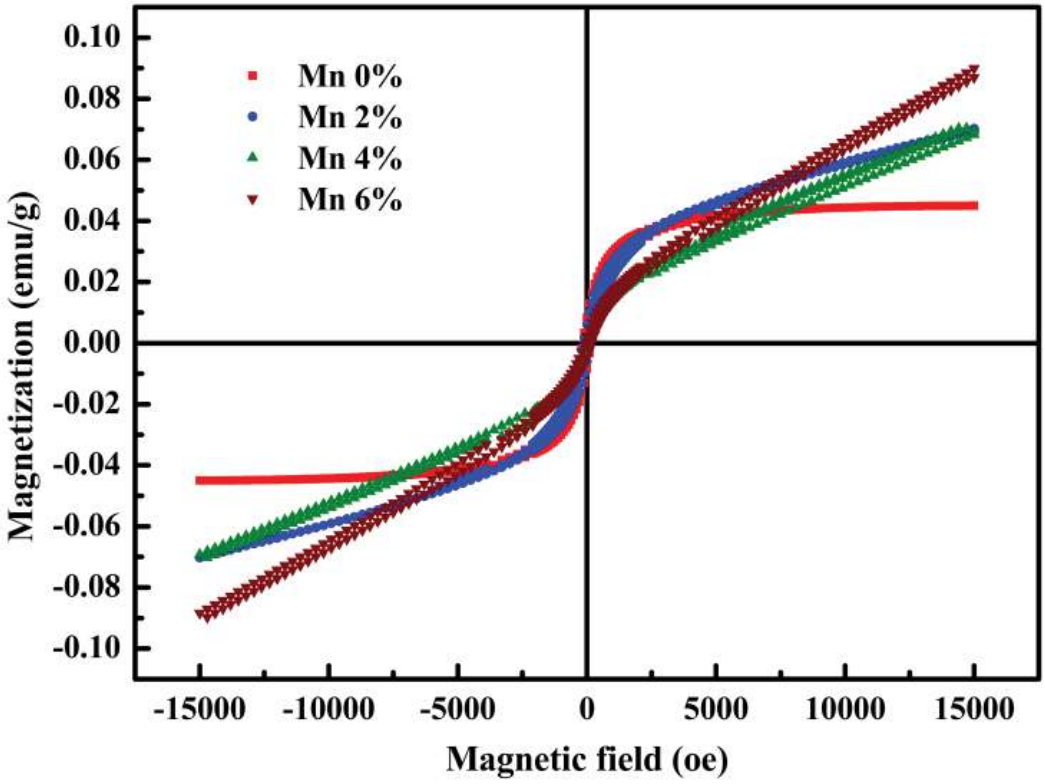

Figure 4.13: M-H curve of pure and Mn doped ZnO nanopowder at 300 K.

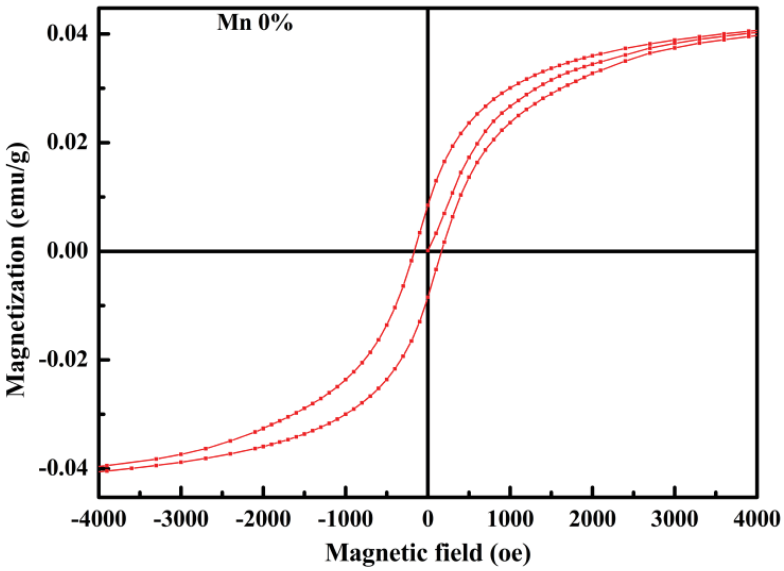

Figure 4.14: M-H curve of pure ZnO nanopowder at 300 K.

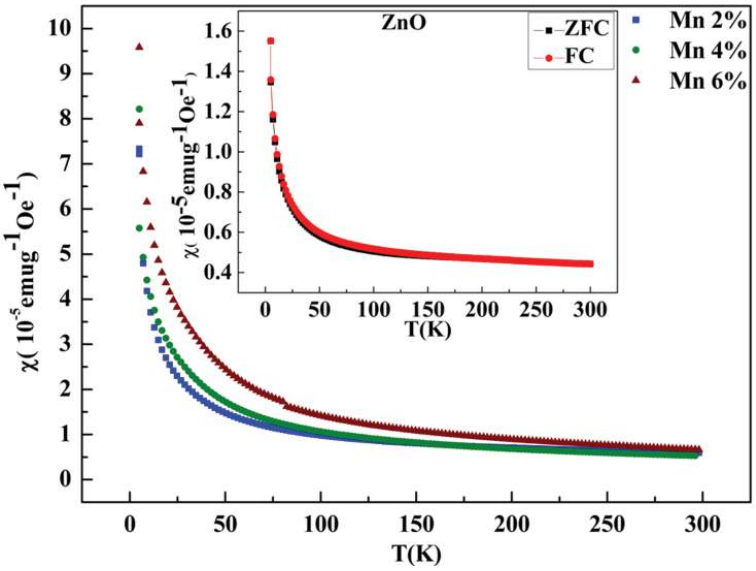

Figure 4.15: Susceptibility curve of Mn doped ZnO. Inset shows ZFC-FC curve of ZnO.

Table 4.5: The H_c , M_{rs} and T_c values of Mn doped ZnO nanopowder			
Mn (at.%)	H_c	M_{rs}	T_c
0	168	0.0084	1257
2	149	0.0061	269
4	148	0.0037	111
6	132	0.0021	80

4.4. CONCLUSION

In this study, we combined XRD, SEM, EDS, UV-VIS, Raman analysis, FTIR, and MPMS as reliable methods to investigate the structural, morphology, elemental, optical and magnetic properties of the Mn doped ZnO. XRD reveals the fact that all samples have single phase and hexagonal wurtzite crystal structure. The shift in XRD peaks towards higher angles and variation in APF, crystallite size, c/a ratio with Mn concentration indicate substitution of Mn ions at Zn site of ZnO lattice. The SEM images confirm the proper grain growth in all the samples. Elemental analysis shows the presence of Zn, Mn and oxygen over the scanned area of the samples. UV-Vis analysis shows that increase in Mn concentration cause shift of absorption edge in visible region and decrease in band gap. Raman analysis has good agreement with XRD results. Some extra peaks in Raman spectra of Mn doped ZnO indicate small lattice distortion in ZnO crystal structure. FTIR study confirms proper incorporation of Mn ions in Zn site of ZnO nanoparticles. Magnetic study indicates presence of RTFM in all the samples. Magnetic behaviour changes with doping concentration due to small lattice distortion and defects. The ferromagnetism in Mn doped ZnO is due to localized magnetic moments mediated by free charge carriers. These localized magnetic moments affects the sp-d exchange interactions by increasing d electron moments of Mn ions, which cause change in the band gap. Therefore optical properties are related to magnetic properties of the samples. The results of XRD, Raman and FTIR indicate that small change in structural property due to Mn incorporation is responsible for observed variation in absorption, band gap and magnetic properties of samples. This indicates that structural, optical and magnetic properties are correlated to each other.